Measurement of the Top Cross Section in the Lepton + Jets Channel Using Simultaneous Kinematic Fits with 2.7 fb^{-1} of CDF Data

The CDF Collaboration
URL http://www-cdf.fnal.gov
(Dated: April 27, 2010)

We measure the top pair production cross section, using data from $p\bar{p}$ collisions at $\sqrt{s} = 1.96$ TeV, with 2.7 ± 0.2 fb^{-1} of data collected by the Collider Detector at Fermilab.

The backgrounds in the b-tagged lepton-plus-jets sample are estimated using a kinematic fit, which simultaneously determines the cross sections and normalizations of $t\bar{t}$, W + jets, QCD, and electroweak processes. This is the first application of a procedure of this kind.

The top cross section is measured to be $\sigma_{t\bar{t}} = 7.64 \pm 0.57(\text{stat} + \text{syst}) \pm 0.45(\text{lumi})$ pb and the Monte Carlo simulation scale factors $K_{Wb\bar{b}} = 1.57 \pm 0.25$, $K_{Wc\bar{c}} = 0.94 \pm 0.79$, $K_{Wc} = 1.90 \pm 0.29$, and $K_{Wq\bar{q}} = 1.10 \pm 0.29$. These results are consistent with existing measurements using other procedures. This approach has an added advantage that many systematic uncertainties are measured in-situ and inversely scale with integrated luminosity similarly to statistical uncertainties.

Preliminary Results for Summer 2010 Conferences

I. INTRODUCTION

Within the context of the Standard Model, in $p\bar{p}$ collisions top quarks are produced in pairs through the strong interaction, via quark annihilation (85%) and gluon fusion (15%) at $\sqrt{s} = 1.96$ TeV. The top quark is expected to decay to a W boson and b quark nearly 100% of the time. The W boson subsequently decays to either a pair of quarks or a lepton-neutrino pair. Measuring the rate of the reaction $p\bar{p} \to t\bar{t} \to \ell\bar{\nu}_\ell qq'b\bar{b}$ tests both the production and decay mechanisms of the top quark.

This note describes a measurement of the top pair production cross section in the lepton+jets channel at $\sqrt{s} = 1.96$ TeV. Backgrounds for this measurement consist of W + heavy flavor, W + light flavor, QCD, and electroweak processes including Z + jets, single top, and di-bosons. One obtains the $t\bar{t}$ cross section from the following formula:

$$\sigma_{t\bar{t}} = \frac{N_{\text{data}} - N_{\text{bkg}}}{\mathcal{A} \cdot L} \tag{1}$$

where N_{data} is the number of observed events that pass the selection criteria, N_{bkg} is the estimated number of background events, $\mathcal{A}$ is the acceptance, and $L = \int \mathcal{L}dt$ is the integrated luminosity. Most methods of calculating the cross section first estimate the small backgrounds, including single top, di-boson, and Z + jets using Monte Carlo simulation (QCD background are estimated from data), leaving W + jets as the only backgrounds.

Run II analyses of the $t\bar{t}$ cross section use a procedure for determining the W + jets backgrounds [1], in which one subtracts the small known backgrounds, leaving the pretag W + jets sample. Next, a "mistag parameterization" (probability that a light jet is b-tagged by mistake) is used to estimate the amount of W + light flavor to have at least one tag. Monte Carlo simulation is used to estimate heavy flavor fractions, and it is compared to another sample to see if extra W + heavy flavor is needed. In the past, the other sample was QCD dijets, but recently, the W+1 and 2 jet bins have been used as these analyses required at least three jets in the event.

Instead of subtracting out the backgrounds, we fit for both the $t\bar{t}$ signal and all backgrounds at once, leading to a more reliable measurement with fewer assumptions in the modeling. This procedure is referred to as the Simultaneous Heavy Flavor and Top Cross Section Measurement (SHyFT). This approach is possible due to both the large CDF dataset and fewer modeling assumptions of the backgrounds. It is similar to the previous technique used at CDF in that both techniques assume that all potential processes that can contribute to the sample are accounted for.

No single variable is able to distinguish between the three main samples in this analysis - the $t\bar{t}$ signal, the W + heavy flavor background and the W + light flavor background. $t\bar{t}$ and W + heavy flavor both contain heavy flavor; W + heavy flavor and W + light flavor both have few jets in the event. But the combination of the number of jets and jet flavor is able to separate these three samples (as well as $Wc/Wc\bar{c}$ + jets). W + heavy flavor has few jets while $t\bar{t}$ has several; $W_{b\bar{b}}$ contains jets with heavy flavor whereas W + light flavor does not. This can be seen in the cartoon shown in Figure 1.
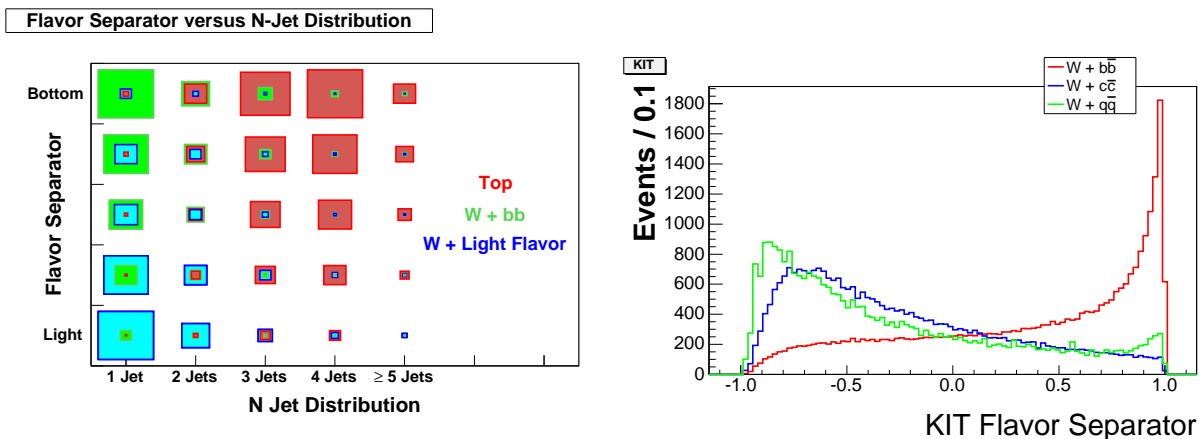

FIG. 1: Left: Cartoon of jet flavor versus n_{jet} for different samples. The size of each box indicates the contribution of the sample to the bin. Each variable on its own is not enough to separate the three samples, but together it is easy to distinguish them. Right: Sample output of the KIT Flavor Separator, showing how different flavors are distinguished from each other. In green is light flavor (u, d jets), in blue is charm flavor, and in red is bottom flavor. Light flavor peaks around -0.9, charm peaks around -0.6, and bottom flavor peaks at 1, providing a good method to distinguish the flavor of a jet.

A flavor separator is an algorithm that provides a single output to determine the flavor of a jet. There are two flavor separators in use at CDF, and both require the jet to be b-tagged with a SECVTX tag, which is a set of requirements

on the tracks and secondary vertex of the jet that is designed to identify the jet as containing a b quark [2]. There are three "operating points" to the SECVTX tagging algorithm — loose, tight, and ultratight — each with a much lower mistag rate but also a lower tagging rate than the previous. We use the Karlsruhe Institute of Technology (KIT) Flavor Separator [3], which is a powerful neural-net based flavor separator, with tight SECVTX tags, because those are what the neural net was initially trained on. An example output of the KIT Flavor Separator is shown in Figure 1.

While both the n_{jet} spectrum and a flavor separator together distinguish the different samples, they are not enough to distinguish parameters that affect those samples. Namely, a change in the top event yield can be due to a different production cross section, or it can be due to a change in the b-tagging efficiency. A change in the b-tagging efficiency affects events with one b-tag differently than those with two tags; a change in the Top cross section affects both identically. To help isolate this differential effect, we use the number of tags as another discriminating factor in the fit.

The flavor-separator distribution of each sample for a given number of jets and b-tags, i.e., a given bin in n_{jet} and n_{tag} (a *jet-tag bin*), is called a *template*. We make templates using the KIT Flavor Separator for signal and background samples after passing them through our event selection (see Section II). The sample used to model QCD is made from data, while all other background samples were generated using Monte Carlo simulation by the Top Group (see Section III). Sample templates are shown in Figure 2. The complete set of templates is shown in Figure 3.
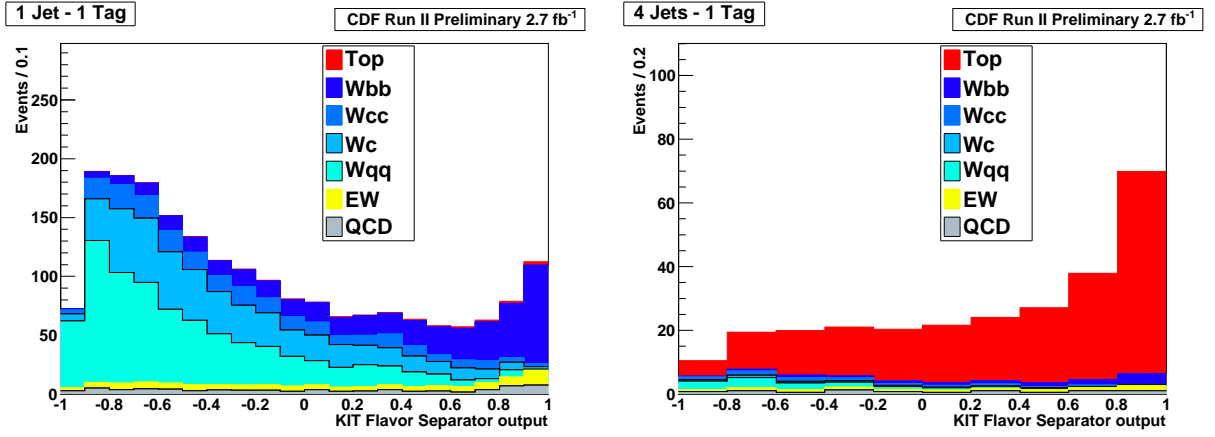

FIG. 2: Sample templates made using the KIT Flavor Separator distribution, in two different jet- and tag-bins. Left: the 1-jet, 1-tag bin. Right: the 4-jet, 1-tag bin.
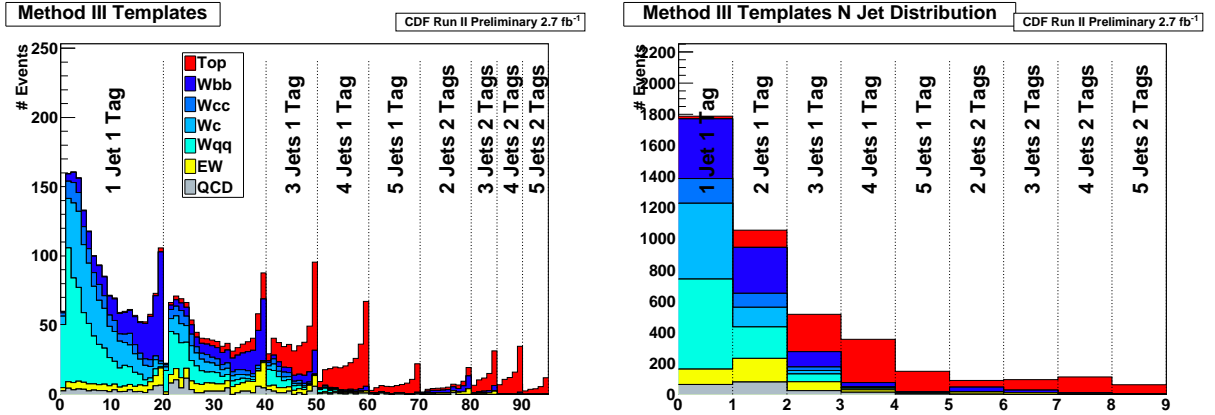

FIG. 3: Left: The complete set of all templates, split by n_{jet} and n_{tag} bins, normalized to the expected yield corresponding to 2.7 fb^{-1} of data. Right: The set of templates projected onto the n_{jet} distribution.

II. DATA SAMPLE & EVENT SELECTION

This analysis is based on a sample of integrated luminosity of 2.7 fb^{-1}, corresponding to data collected from February 2002 through April 2008 using the CDF II detector [4]. The data was collected with triggers that require a high-p_T (18 GeV/c) electron or muon.

The criteria required in order for an event to be considered "good" is designed so that only top events are analyzed. Ordinarily, these event selection criteria would be optimized for that effect. In this analysis, however, we start with the standard lepton-plus-jets selection (as shown in Table I) and add a QCD veto cut but do not make any further optimization. This is because we fit for the backgrounds in the non-signal region and to estimate them in the signal region.

TABLE I: Selection criteria for the lepton-plus-jets channel.

Variable	Selection Criteria
n$_{jet}$	≥ 1
Jet E_T	$\geq$ 20 GeV/c^2
Jet $|\eta|$	$<$ 2.0
Lepton	1 CEM electron, or CMUP or CMX muon
Lepton E_T	$\geq$ 20 GeV/c^2
n$_{tag}$	$\geq$ 1 Tight SECVTX tag

The QCD backgrounds are extremely difficulty to model, so it is advantageous to simply remove as much of the QCD contribution as possible. This is done using a QCD Veto, which makes cuts on the transverse mass of the W,

$$m_T^W = \sqrt{2(p_T^\ell p_T^\nu - p_x^\ell p_x^\nu - p_y^\ell p_y^\nu)} \tag{2}$$

and the MET Significance (MetSig),

$$MetSig = \frac{\not{E}_T}{\sqrt{\overrightarrow{E}_T^{\,\mathrm{uncl}} \cdot \hat{\not{E}}_T}} \tag{3}$$

The QCD elimination cuts and final selection criteria are shown in Table II.

TABLE II: Event selection criteria. The last three cuts together form the QCD Veto.

Variable	Selection Criteria
$\not{E}_T$	$\geq$ 20 GeV
n$_{tag}$	1 or 2
Run	Good silicon
m_T^W	$>$ 10 GeV/c^2 for muons
m_T^W	$>$ 20 GeV/c^2 for electrons
$MetSig$	$> (-0.05 m_T^W + 3.5)$ for electrons

III. SIGNAL AND BACKGROUND MODELING

We estimate our signal contribution and most of the background contributions using Monte Carlo simulation. The signal Monte Carlo simulation sample was generated using PYTHIA v6.216 [5], assuming a top mass of $m_t = 175$ GeV/c^2. The sample was generated corresponding to the data yield of 2.7 fb^{-1}, but is stored as 1 fb^{-1} statistics for convenience. Indeed, all of our signal and background samples are stored in this manner. All non-QCD Monte Carlo simulation samples were generated using PYTHIA v6.216; MadGraph [6]; or ALPGEN v2.10$'$ [7] with generator-to-reconstructed-jet matching[8][9] and PYTHIA v6.326 for showering.

A. W + Jets

W + heavy flavor backgrounds consist of $Wb\bar{b}$ + jets, $Wc\bar{c}$ + jets, and Wc + jets, as well as $Wq\bar{q}$ + jets that contains any heavy flavor. All W + jets samples are normalized by a fixed scale factor, S$_{\sigma_W}$, to compensate for

the difference between the true ('all orders') W + jets production cross section and the cross section from ALPGEN (which is leading-order with some corrections), and is given by

$$S_{\sigma_W} = \frac{\sigma_{W_{true}}}{\sigma_{W_{ALPGEN}}} = 1.35 \qquad (4)$$

W + light flavor backgrounds consist of W + jets events with no heavy flavor. As with the W + heavy flavor backgrounds, these light flavor backgrounds also have the same scale factor, S_{σ_W}, given by Equation 4.

The Monte Carlo simulation samples for the W + light flavor backgrounds have some heavy flavor contributions, due to the appearance of $b\bar{b}$ and $c\bar{c}$ pairs in the modeling of hadronization (via gluon splitting). These must be taken care of by a heavy flavor overlap removal algorithm. In our case, we remove any events which were double counted, and move any remaining events with heavy flavor to the appropriate W + heavy flavor template.

B. QCD

While much of the QCD background was eliminated with the QCD Veto (see Section II), some remains and must be estimated. "Anti-electrons" are electron candidates that pass the same kinematic electron cuts as our signal sample but fail two of the electron ID cuts [10]. This ensures they are not identified as electrons, and thus do not come from W decays; because the QCD cross section is so large, it is assumed that QCD dominates the anti-electron sample. Anti-electrons model the shape of the QCD background distribution well, but its normalization is different due to changes in the electron ID cuts and thus needs to be estimated separately.

To the flavor-separator distribution we apply a scale factor, S_{QCD}, calculated by fitting the $\not{E}_T$ distributions from anti-electrons and W + jets to the data. Applying the full selection criteria to the anti-electron sample would yield too few events for a proper fit; instead, the n_{tag} requirement is not applied (the $\not{E}_T$ is also excluded), which leads the unscaled shape distributions to have equal normalizations in the same jet-bin (e.g., the 2-jet, 1-tag and 2-jet, 2-tag distributions have the same unscaled normalization). Because the fit is made to data with the n_{tag} requirement, however, the resulting scale factor is applied only to the QCD template for that particular jet-tag bin. Figure 4 shows the $\not{E}_T$ distribution for the 1-jet 1-tag bin from which the S_{QCD} is obtained.
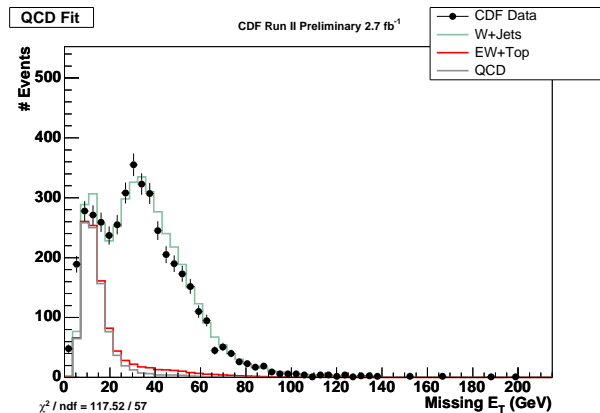

FIG. 4: $\not{E}_T$ fit of QCD and W + jets to the data for the 1-jet 1-tag bin. From this, the S_{QCD} for that jet and tag bin is obtained. Note that a large fraction of the QCD distribution lies below the $\not{E}_T \leq$ 20 GeV cut we apply.

C. Other Electroweak Processes

The other electroweak processes we consider as backgrounds for this analysis include single top (both s- and t-channel), di-boson (WW, WZ, ZZ), and Z + jets. Similar to the W + jets events above, the Z + jets samples need to be rescaled by a 'K-factor' to take into account contributions from higher-order processes that are not included in ALPGEN. We use $K = 2.0$ for the Z + heavy flavor samples and $K = 1.4$ for Z + light flavor samples [11], and these are not allowed to float in the fit.

D. Mistags

All of the Monte Carlo simulation samples, including our top signal sample, have the potential of one or more light flavor jets being mistakenly tagged as a b-jet (a *mistag*). Unfortunately, the tagging algorithm applied during the simulation does a poor job of modeling the observed mistag rate. We apply a separate algorithm called the *mistag parameterization* to re-scale the shapes of all flavor-separator distributions produced by the Monte Carlo simulation so that they agree with the observed mistag rate.

IV. FITTER

The fitter is a binned Poisson likelihood fitter, based on the MINUIT package. The set of templates for all samples are combined to form probability density functions, by normalizing them to the predicted yield for 2.7 fb^{-1}, where the normalization factors are functions of other physical quantities (cross sections and various scale factors), which are all parameters in the fit. The normalizations also include functions $P_N^x(i, j, R_x)$ that parameterize the source of systematic uncertainties x with respect to the number of tags, i, number of jets, j, and the relative shift of the uncertainty, R_x. For example, the functional form for the uncertainty due to the Jet Energy Scale is given by $P_N^{JES}(i, j, R_{JES})$. We use $P_N^{Btag}(i, j, R_{Btag})$, $P_N^{Mistag}(i, j, R_{Mistag})$, $P_N^{JES}(i, j, R_{JES})$, $P_N^{I/FSR}(i, j, R_{I/FSR})$, and $P_N^{Q^2}(i, j, R_{Q^2})$ to parameterize the effects the b-tagging rate, the mistag rate, the Jet Energy Scale, Initial- and Final-State Radiation, and the Q^2 energy scale, respectively. Two visualizations of these parameterizations are given in Figure 5.
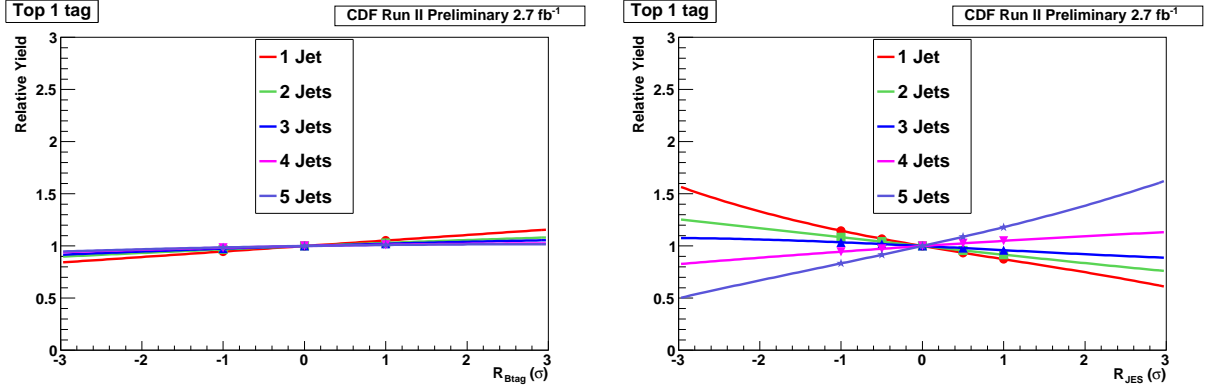

FIG. 5: Examples of the functional forms of the template normalization as systematic effects are shifted. Left: The b-tag uncertainty in the Top single tag templates. Right: The JES uncertainty in the Top single tag templates.

The total normalizations of each sample are given in Equations 5 – 11.

$$N_{t\bar{t}}^{pred}(i,j) = \sigma_{t\bar{t}} \cdot N_{t\bar{t}}^{MC}(i,j) \cdot w_{ALP} \cdot \epsilon_{lep} \cdot L \cdot \mathcal{B}(i,j) \cdot P_N^{I/FSR}(i,j,R_{I/FSR}) \cdot$$
$$P_N^{Btag}(i,j,R_{Btag}) \cdot P_N^{Mistag}(i,j,R_{Mistag}) \cdot P_N^{JES}(i,j,R_{JES}) \tag{5}$$

$$N_{Wb\bar{b}}^{pred}(i,j) = K_{Wb\bar{b}} \cdot N_{Wb\bar{b}}^{MC}(i,j) \cdot w_{ALP} \cdot \epsilon_{lep} \cdot L \cdot S_{\sigma_W} \cdot \mathcal{B}(i,j) \cdot$$
$$P_N^{Btag}(i,j,R_{Btag}) \cdot P_N^{Mistag}(i,j,R_{Mistag}) \cdot P_N^{JES}(i,j,R_{JES}) \cdot P_N^{Q^2}(i,j,R_{Q^2}) \tag{6}$$

$$N_{Wcc}^{pred}(i,j) = K_{Wc\bar{c}} \cdot N_{Wcc}^{MC}(i,j) \cdot w_{ALP} \cdot \epsilon_{lep} \cdot L \cdot S_{\sigma_W} \cdot \mathcal{B}(i,j) \cdot$$
$$P_N^{Btag}(i,j,R_{Btag}) \cdot P_N^{Mistag}(i,j,R_{Mistag}) \cdot P_N^{JES}(i,j,R_{JES}) \cdot P_N^{Q^2}(i,j,R_{Q^2}) \tag{7}$$

$$N_{Wc}^{pred}(i,j) = K_{Wc} \cdot N_{Wc}^{MC}(i,j) \cdot w_{ALP} \cdot \epsilon_{lep} \cdot L \cdot S_{\sigma_W} \cdot \mathcal{B}(i,j) \cdot$$
$$P_N^{Btag}(i,j,R_{Btag}) \cdot P_N^{Mistag}(i,j,R_{Mistag}) \cdot P_N^{JES}(i,j,R_{JES}) \cdot P_N^{Q^2}(i,j,R_{Q^2}) \tag{8}$$

$$N_{Wqq}^{pred}(i,j) = K_{Wq\bar{q}} \cdot N_{Wqq}^{MC}(i,j) \cdot w_{ALP} \cdot \epsilon_{lep} \cdot L \cdot S_{\sigma_W} \cdot \mathcal{B}(i,j) \cdot$$
$$P_N^{Mistag}(i,j,R_{Mistag}) \cdot P_N^{JES}(i,j,R_{JES}) \cdot P_N^{Q^2}(i,j,R_{Q^2}) \tag{9}$$

$$N_{EW}^{pred}(i,j) = K_{EW} \cdot N_{EW}^{MC}(i,j) \cdot w_{ALP} \cdot \epsilon_{lep} \cdot L \cdot \mathcal{B}(i,j) \cdot$$
$$P_N^{Btag}(i,j,R_{Btag}) \cdot P_N^{Mistag}(i,j,R_{Mistag}) \cdot P_N^{JES}(i,j,R_{JES}) \tag{10}$$

$$N_{QCD}^{pred}(i,j) = K_{QCD} \cdot N_{QCD}^{MC}(i,j) \cdot S_{QCD}(i,j) \tag{11}$$

V. SOURCES OF SYSTEMATIC UNCERTAINTIES

Systematic uncertainties in this measurement can affect both the normalizations of each jet-tag bin as well as the shapes of the templates. These are manifested through the fitter. There are other uncertainties that affect the measurement by a set percentage. They are dealt with in different manners.

For the rate uncertainties, we generate additional sets of templates with the variable in question shifted up and down. The relative differences in event yields are interpolated to yield the functional parameterizations described in Section IV. For shape uncertainties, we again generate an additional set of templates with the variable in question shifted, and then re-run the fit with those templates in place of the nominal ones. We take the difference in the result as the uncertainty.

Initial- and Final-State Radiation (I/FSR) are processes in which gluons are radiated before or after the collision, respectively. Regardless of when they are radiated, the uncertainty arises due to I/FSR leading to a larger or smaller number of jets in the event. To account for this, we make additional sets of templates with more or less ISR and FSR as compared to the normal settings.

A series of corrections is applied to the raw energy measured from the calorimeters in order to estimate the true energy of the jet [12]. These corrections are necessary to account for various detector effects, such as calibration, η and ϕ dependence, et cetera. The uncertainties of each correction are convoluted together to yield an overall uncertainty, σ, on the energy of the jet called the Jet Energy Scale (JES). We account for this uncertainty by varying the JES on all Monte Carlo simulation-based samples to four different points: $\pm 0.5\,\sigma$ and $\pm 1\,\sigma$.

Decreasing the Q^2 energy scale effectively increases the value of α_s, leading to an enhanced radiative production of additional partons. This increased production in turn leads to more jets. We account for this possibility by varying the Q^2 energy scale of the $W +$ jets templates to 0.5 and 2.0.

Both the b-tagging efficiency and the mistag matrix used to model the tagging rates in simulation have uncertainties associated with them. In order to account for these uncertainties, we vary the b-tagging efficiency by 1σ and the mistag rate by 20%.

The models used to shower partons in the Monte Carlo simulation are not known accurately, and so we run the fit with a different showering model, HERWIG than the default. We account for uncertainties in our modeling of the QCD shape by using jet-electrons to make templates, instead of the default anti-electrons. Similar to anti-electrons, jet-electrons are jets which appear to be electrons. The KIT Flavor Separator has a correction factor applied to match its mistag rate to the one observed in data; to account for this uncertainty, we examine templates without this factor applied. The models to describe color reconnection are not known precisely, and so we account for this uncertainty by comparing two different models: the so-called Apro and ACRpro.

As we use the same event selection as in previous analyses, which re-weighted the top sample using the CTEQ6L parton distribution function [13], we simply take the same fractional uncertainty of 4% on the top cross section. The measured luminosity has an uncertainty of 5.9%, and so we take the same uncertainty on our top cross section result.

VI. RESULTS

The results we obtain from the fitter are twofold: a set of normalizations for the templates (which give the $t\bar{t}$ cross section and W + jets K-factors) and a set of relative shifts for the systematic uncertainties that together minimize the negative log likelihood when those templates are fit to the data; and a visual representation of that fit to the data.

The fit to the data is shown in Figures 6 and 7. The normalizations from the fit are shown in Table III. The top cross section result is given in picobarns, whereas the W + jets, EW, and QCD results are given as K-factors, relative to the default normalizations used in this analysis. The results for the systematic uncertainties are shown as shifts relative to the default values used. The normalizations we obtain are similar to those obtained from other procedures.
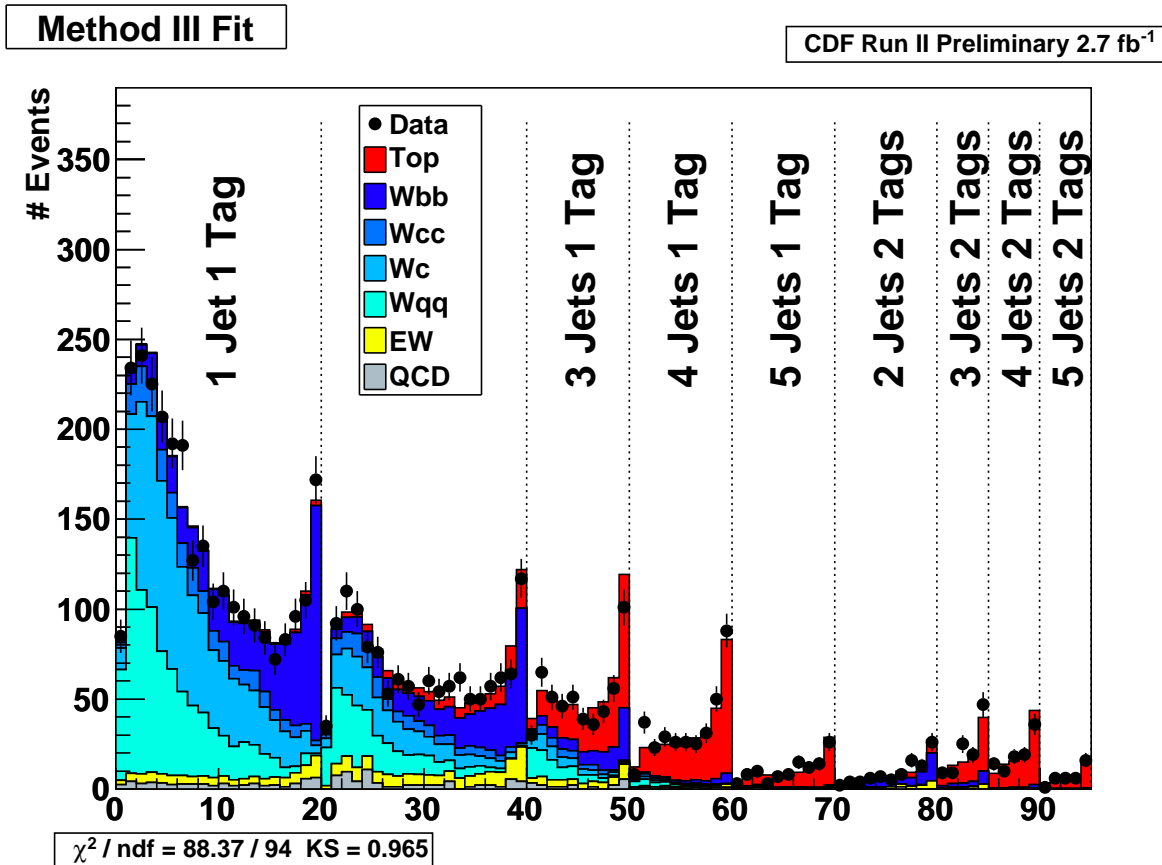
FIG. 6: The templates after being fit to the data, split by n_{jet} and n_{tag} bins.

VII. COMPARISON TO THE PREVIOUS METHOD

As the main impetus for this measurement technique is an improvement on uncertainties, we wish to compare them to an analysis using the current procedure. In order to do that, we must extract individual uncertainties from the fit and we run the fit twice to do that. The fitter is run first with no systematics included, yielding the statistics-only uncertainty, and second with only the uncertainty in question included. The uncertainties from the two fit results are subtracted in quadrature to yield the single systematic uncertainty. Because the fitter determines the uncertainties concurrently, this is only an estimate of an individual uncertainty, and only calculated for comparison purposes.

Shown in Table IV is a comparison of the uncertainties from this analysis to an analysis using the same amount of data and assumed top mass [13], but which uses a different method to estimate the backgrounds. This analysis has improved on almost every uncertainty. The only exception is the uncertainty due to the Jet Energy Scale, which remained the same. The uncertainties determined concurrently in the fitter in this analysis are denoted with asterisks.
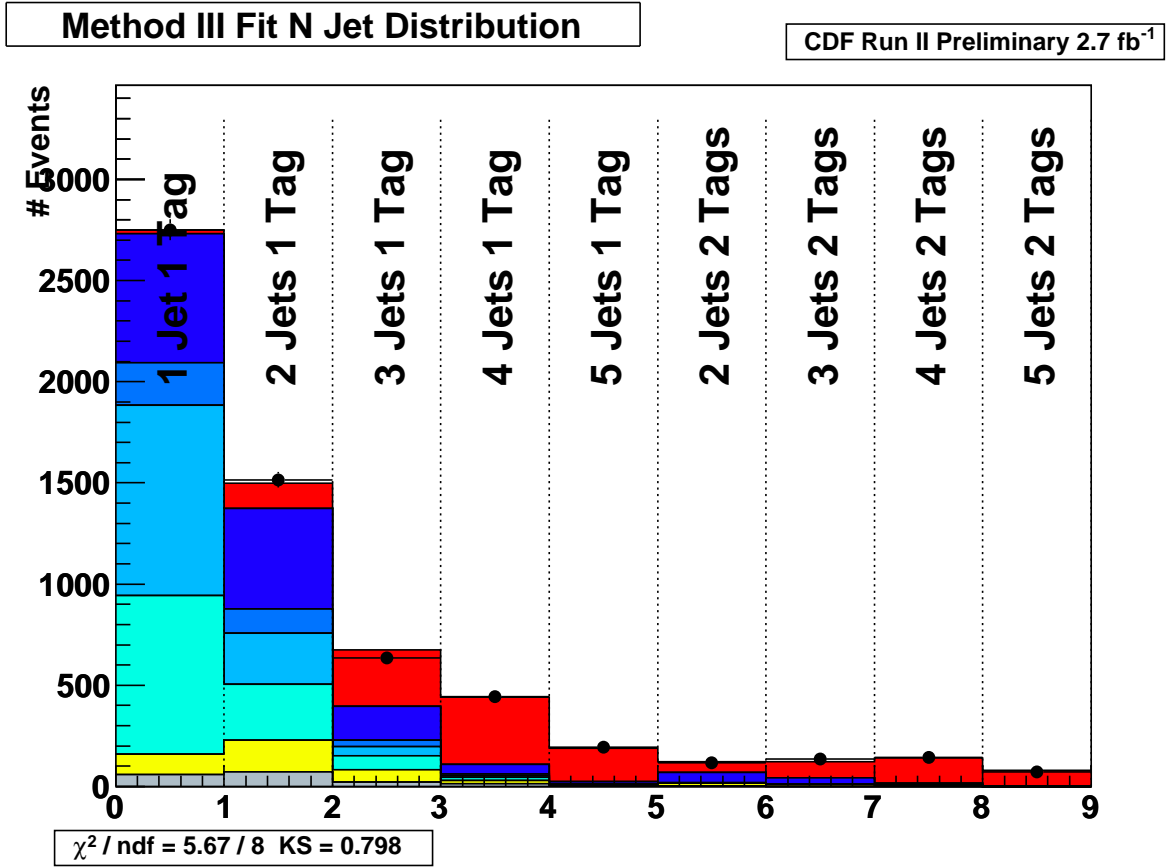
FIG. 7: The templates after being fit to the data, projected onto the n_{jet} distribution

TABLE III: Normalizations for each sample as determined by the fit. The top cross section is quoted in picobarns, whereas the W + jets, electroweak, and QCD results are given as k-factors. The systematic uncertainty results are given as relative shifts.

Sample	Fit Value
$\sigma_{t\bar{t}}$	$7.64^{+0.57}_{-0.54}$
$K_{Wb\bar{b}}$	$1.57^{+0.28}_{-0.22}$
$K_{Wc\bar{c}}$	$0.94^{+0.90}_{-0.71}$
K_{Wc}	$1.90^{+0.34}_{-0.32}$
$K_{Wq\bar{q}}$	$1.10^{+0.34}_{-0.25}$
K_{EW}	$1.10^{+0.10}_{-0.10}$
K_{QCD}	$0.82^{+0.26}_{-0.26}$
R_{Btag}	$0.31^{+0.64}_{-0.64}$
R_{Mistag}	$-0.05^{+0.98}_{-0.98}$
R_{JES}	$0.47^{+0.63}_{-0.61}$
R_{Q^2}	$0.07^{+0.44}_{-0.44}$
R_{IFSR}	$0.13^{+0.90}_{-0.89}$

Appendix A: Kinematic Validation Plots

Using the normalizations returned by the fitter, we made plots of kinematic quantities to validate our modeling of the signal and background. These are shown in Figures 8 – 17. We don't see any major discrepancies.

TABLE IV: Comparison of uncertainties from this analysis and a previous one using the same amount of data, but a different background estimation method. Values are given in picobarns. The uncertainties marked with an asterisk are included for comparison only. Note that this analysis includes the Heavy Flavor Correction as part of the statistical uncertainty. The previous analysis did not use the KIT Flavor Separator, and so does not have an uncertainty associated with its correction. Finally, the previous analysis did not estimate an uncertainty due to the Q^2 energy scale.

Uncertainty	This Analysis	Previous Analysis
Statistical	0.33	0.36
Heavy Flavor Correction	—	0.27
Jet Energy Scale*	0.29	0.29
b-Tagging*	0.23	0.39
Mistags*	0.08	0.17
Q^2*	0.21	—
ISR/FSR*	0.01	0.06
Luminosity	0.45	0.43
QCD Shape	0.01	0.06
Parton Showering	0.11	0.21
KIT Correction	0.10	—
Color Reconnection	0.03	—
Lepton ID	0.05	0.04
Z_0	0.02	0.02
PDF	0.05	0.04
Total	0.73	0.84
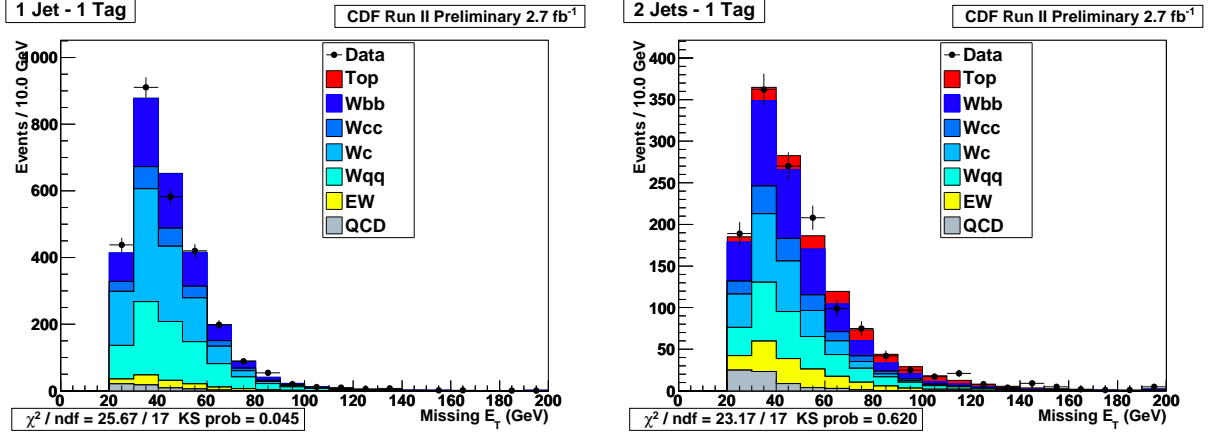
FIG. 8: Kinematic validation plots of the missing transverse energy, in two different jet- and tag-bins. Left: the 1-jet, 1-tag bin. Right: the 2-jet, 1-tag bin.
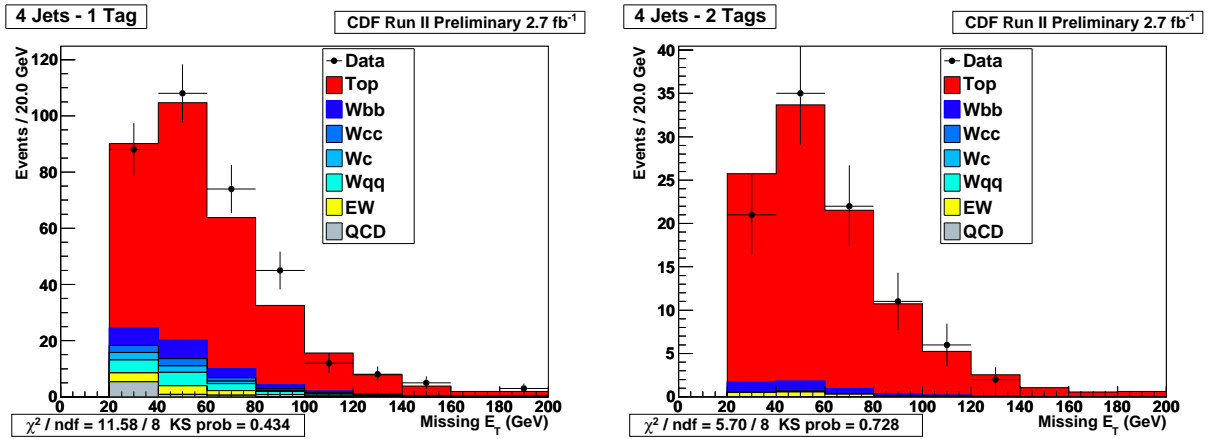

FIG. 9: Kinematic validation plots of the missing transverse energy, in two different jet- and tag-bins. Left: the 4-jet, 1-tag bin. Right: the 4-jet, 2-tag bin.
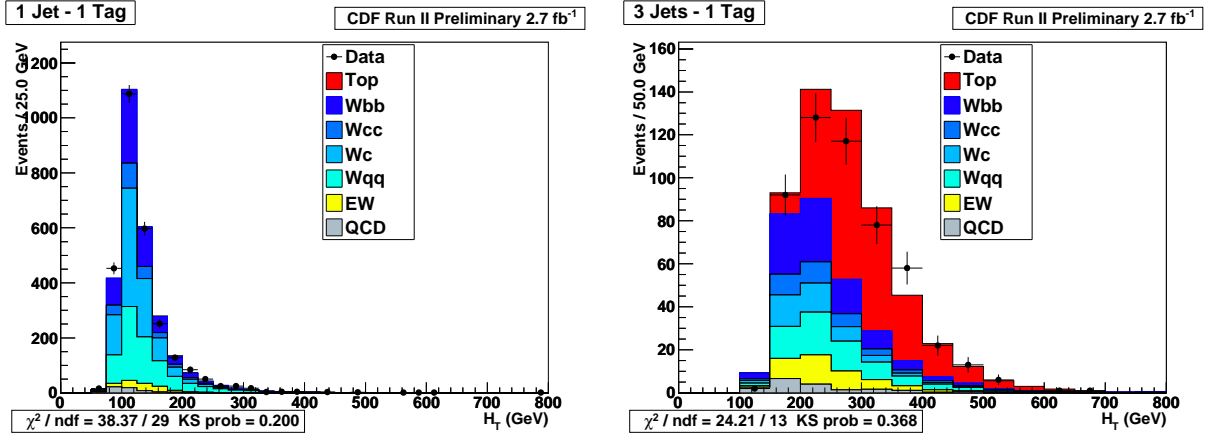
FIG. 10: Kinematic validation plots of the total transverse energy, in two different jet- and tag-bins. Left: the 1-jet, 1-tag bin. Right: the 3-jet, 1-tag bin.
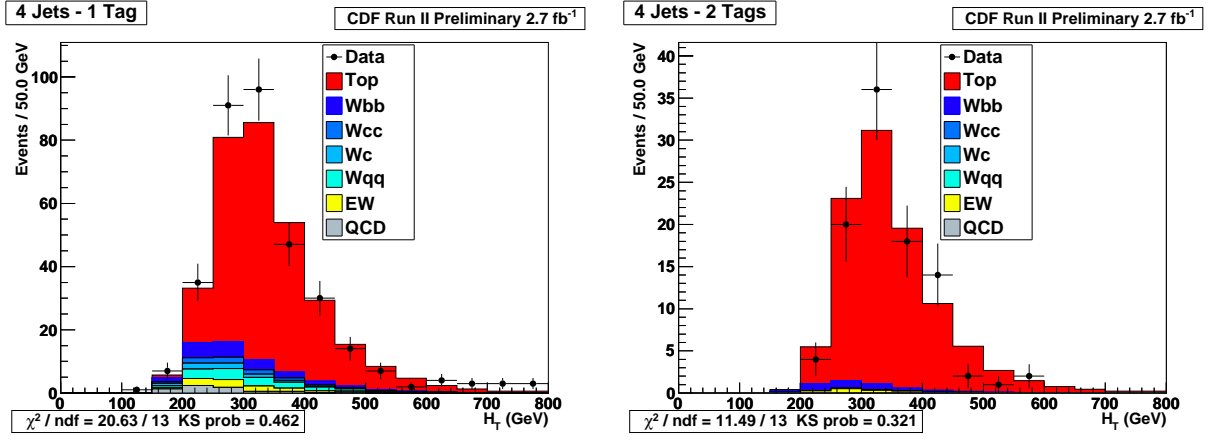

FIG. 11: Kinematic validation plots of the total transverse energy, in two different jet- and tag-bins. Left: the 4-jet, 1-tag bin. Right: the 4-jet, 2-tag bin.
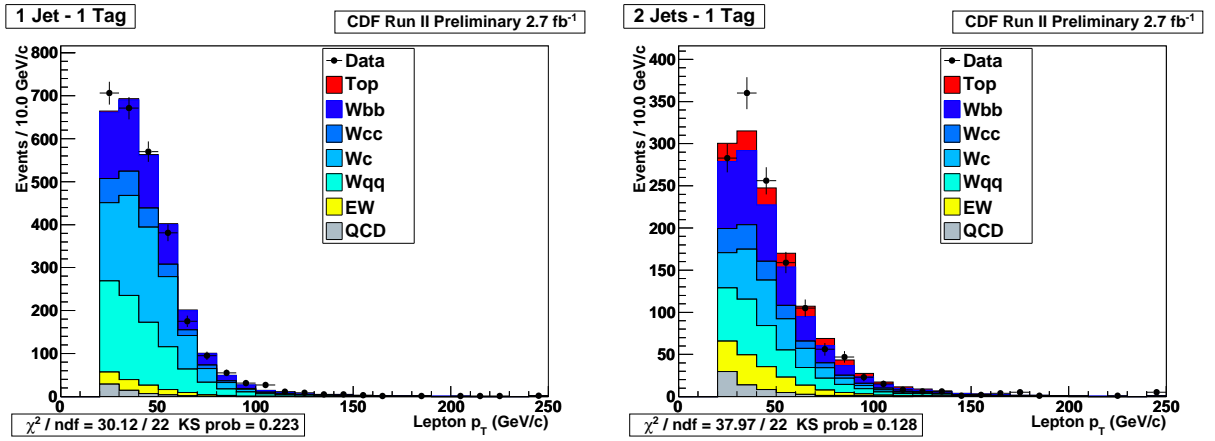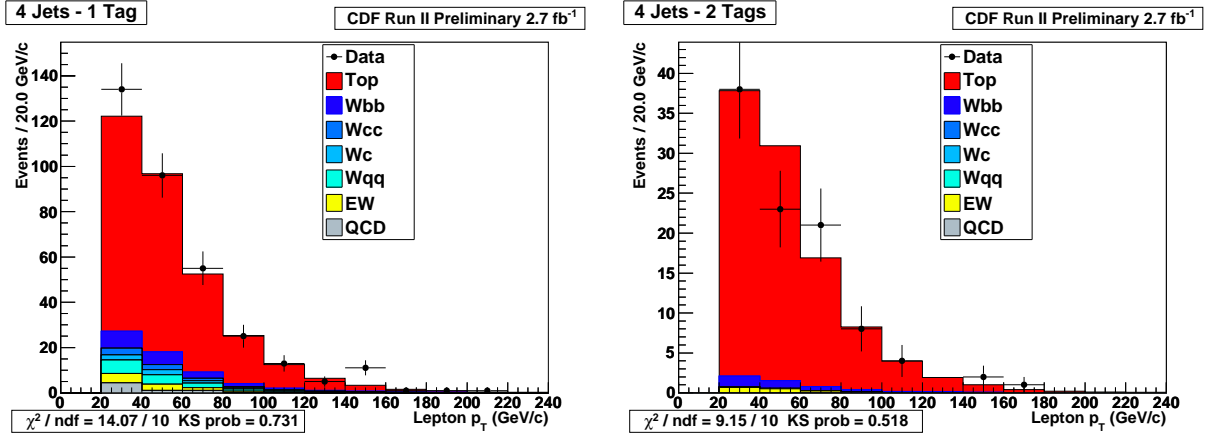

FIG. 12: Kinematic validation plots of the transverse momentum of the lepton, in two different jet- and tag-bins. Left: the 1-jet, 1-tag bin. Right: the 3-jet, 1-tag bin.

FIG. 13: Kinematic validation plots of the transverse momentum of the lepton, in two different jet- and tag-bins. Left: the 4-jet, 1-tag bin. Right: the 4-jet, 2-tag bin.
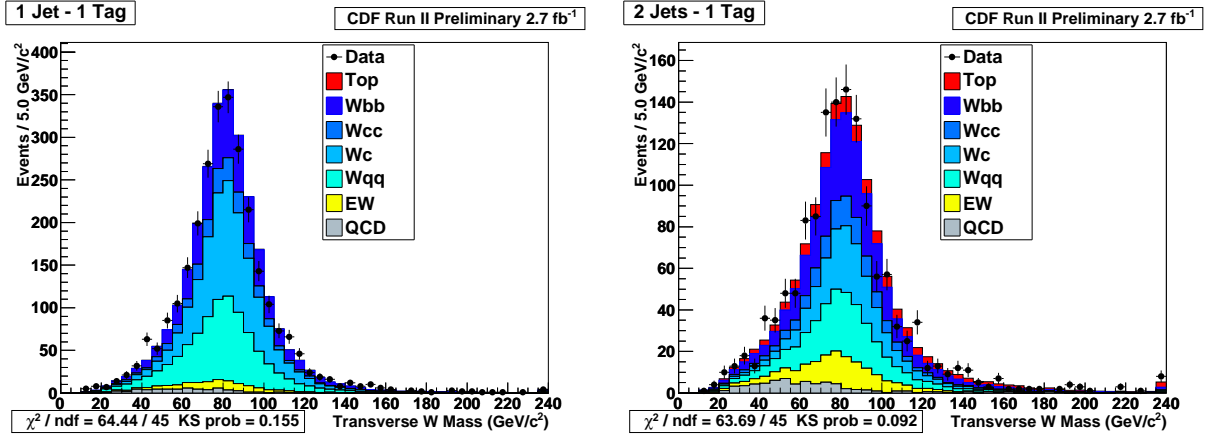

FIG. 14: Kinematic validation plots of the invariant transverse mass of the leptonic W boson, in two different jet- and tag-bins. Left: the 1-jet, 1-tag bin. Right: the 2-jet, 1-tag bin.
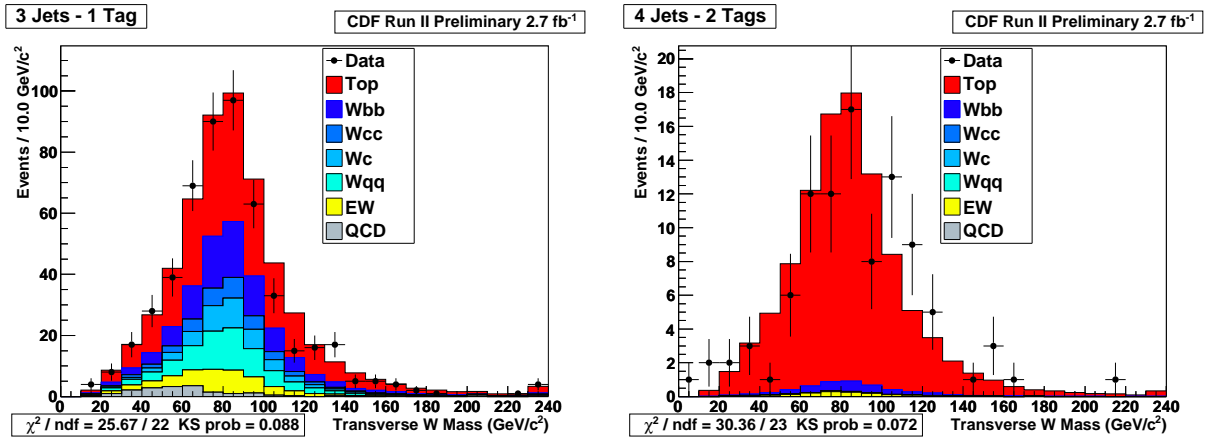

FIG. 15: Kinematic validation plots of the invariant transverse mass of the leptonic W boson, in two different jet- and tag-bins. Left: the 3-jet, 1-tag bin. Right: the 4-jet, 2-tag bin.
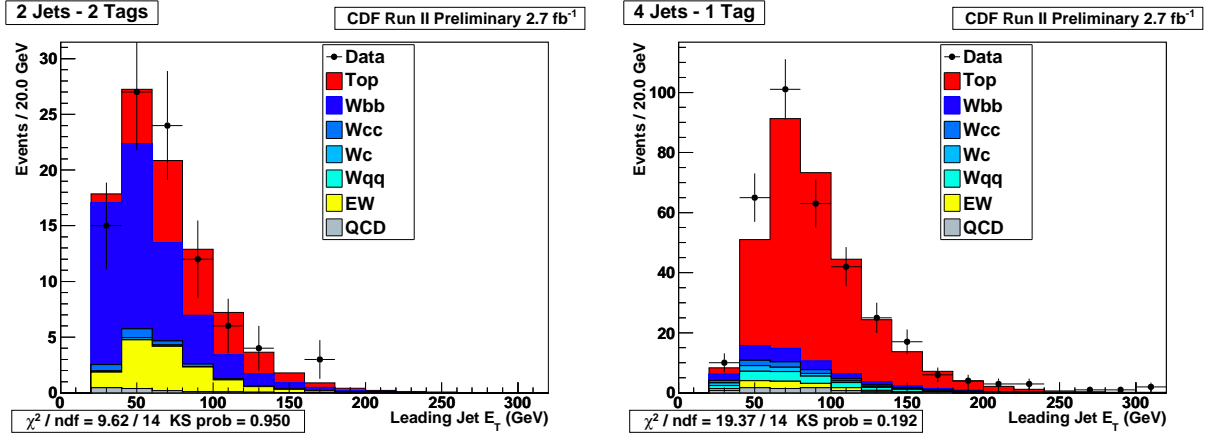
FIG. 16: Kinematic validation plots of the transverse energy of the first jet, in two different jet- and tag-bins. Left: the 2-jet, 2-tag bin. Right: the 4-jet, 1-tag bin.
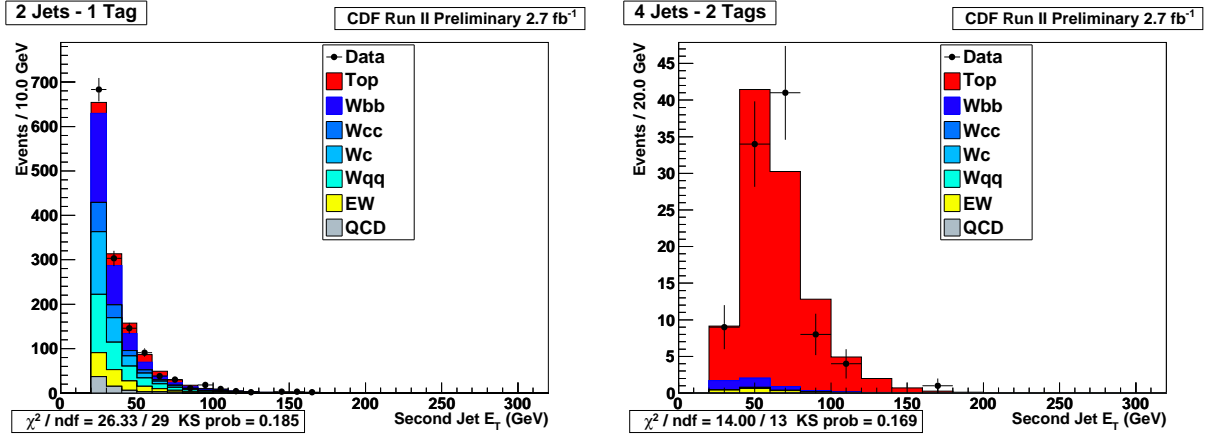

FIG. 17: Kinematic validation plots of the transverse energy of the second jet, in two different jet- and tag-bins. Left: the 2-jet, 1-tag bin. Right: the 4-jet, 2-tag bin.
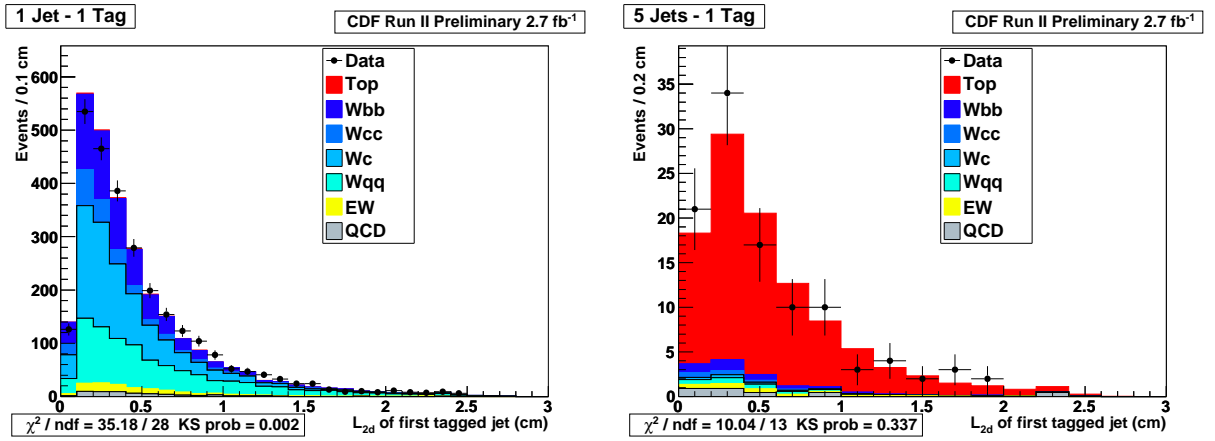

FIG. 18: Kinematic validation plots of the two-dimensional displacement of the first tagged jet, in two different jet- and tag-bins. Left: the 1-jet, 1-tag bin. Right: the 5-jet, 1-tag bin.
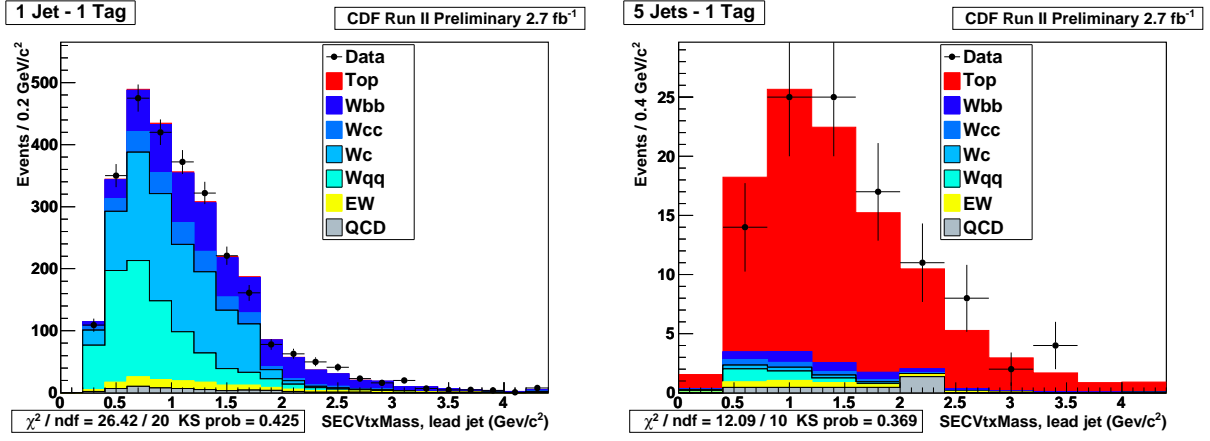
FIG. 19: Kinematic validation plots of the secondary vertex mass of the first tagged jet, in two different jet- and tag-bins. Left: the 1-jet, 1-tag bin. Right: the 5-jet, 1-tag bin.

[1] D. Acosta et al. (CDF Collaboration), *Measurement of the $t\bar{t}$ Production Cross Section in $p\bar{p}$ Collisions at $\sqrt{s} = 1.96$ TeV Using Lepton + Jets Events with Secondary Vertex b-Tagging*, Phys. Rev. **D71** (2005), 052003.

[2] D. Acosta et al. (CDF Collaboration), *Measurement of $t\bar{t}$ Production Cross Section in $p\bar{p}$ Collisions at $\sqrt{s} = 1.96$ TeV Using Lepton + Jets Events with Secondary Vertex b-Tagging*, Phys. Rev. D. **D71** (2005), 052003.

[3] S. Richter (CDF Collaboration), *Search for the Electroweak Single Top-Quark Production with the CDF II Experiment*, Ph.D. thesis, Universität Karlsruhe, 2007.

[4] D. Acosta et al. (CDF Collaboration), *Measurement of the J/ψ Meson and b-Hadron Production Cross Sections in $p\bar{p}$ Collisions at $\sqrt{s} = 1960$ GeV*, Phys. Rev. **D71** (2005), 032001.

[5] T. Sjostrand, L. Lonnblad, S. Mrenna, and P. Skands, PYTHIA *6.3 Physics and Manual*, 2003.

[6] J. Alwall et al., *MadGraph/MadEvent v4: The New Web Generation*, JHEP **09** (2007), 028.

[7] M. Mangano, M.and Moretti, F. Piccinini, R. Pittau, and A. Polosa, *ALPGEN, a generator for hard multiparton processes in hadronic collisions*, JHEP **07** (2003), 001.

[8] J. Alwall et al., *Comparative Study of Various Algorithms for the Merging of Parton Showers and Matrix Elements in Hadronic Collisions*, Eur. Phys. J. **C53** (2008), 473–500.

[9] M. L. Mangano, M. Moretti, F. Piccinini, and M. Treccani, *Matching Matrix Elements and Shower Evolution for Top-Quark Production in Hadronic Collisions*, JHEP **0701** (2007), 013.

[10] B. Cooper and A. Messina (CDF Collaboration), *Estimation of the Background to $W^{\pm} \rightarrow e^{\pm}\nu + n$ Jet Events*, /CDF/PHYS/JET/PUBLIC/7760 (2005).

[11] T. Altonen et al. (CDF Collaboration), *Measurement of Cross Sections for b Jet Production in Events with a Z Boson in $p\bar{p}$ Collisions at $\sqrt{s} = 1.96$ TeV*, Phys. Rev. **D79** (2009), 052008.

[12] A. Bhatti et al., *Determination of the Jet Energy Scale at the Collider Detector at Fermilab*, Nucl. Instrum. Meth. **A566** (2006), 375–412.

[13] T. Schwarz, A. Ivanov, and R. Erbacher (CDF Collaboration), *Measurement of the Top Pair Cross Section in the Lepton Plus Jets Decay Channel with $2.7\,\mathrm{fb}^{-1}$* , /CDF/PUB/TOP/PUBLIC/9462 (2008).